Journal of Molecular Graphics and Modelling 27 (2008) 45–58

Contents lists available at ScienceDirect

Journal of Molecular Graphics and Modelling

journal homepage: www.elsevier.com/locate/JMGM

Molecular mechanics and molecular orbital simulations on specific interactions between peroxisome proliferator-activated receptor PPARα and plasticizer

Tomohiko Nakagawa [a], Noriyuki Kurita [b,*], Shinsaku Kozakai [b], Shingo Iwabuchi [b], Yoko Yamaguchi [b], Masato Hayakawa [b], Yuki Ito [a], Toshifumi Aoyama [c], Tamie Nakajima [a]

[a] Department of Occupational Environmental Health, Nagoya University, Graduate School of Medicine, 65 Tsurumaicho, Showa-ku, Nagoya 446-8550, Japan
[b] Department of Knowledge-Based Information Engineering, Toyohashi University of Technology, Tempaku-cho, Toyohashi, Aichi 441-8580, Japan
[c] Department of Aging Metabolic Regulation, Institute on Aging and Adaptation, Shinshu University, Graduate School of Medicine, 3-1-1 Asahi, Matsumoto, Nagano 390-8621, Japan

ARTICLE INFO

Article history:
Received 7 January 2008
Received in revised form 19 February 2008
Accepted 19 February 2008
Available online 23 February 2008

Keywords:
Peroxisome proliferator-activated receptor
Phthalate esters
Molecular simulations
Molecular mechanics method
Molecular orbital method
Electronic properties
Ligand binding affinity

ABSTRACT

Peroxisome proliferator-activated receptor α (PPARα) has various physiological functions such as lipid and glucose metabolism, inflammation and fibrosis in living organisms. Many types of ligand molecules such as phthalate and adipate esters control these physiological functions. In the present study, to elucidate the dependence of PPARα properties on ligand binding, we investigated stable structures and electronic properties for the complexes of PPARα and phthalate as well as adipate esters, which are used as a plasticizer, by molecular simulations based on molecular mechanics and molecular orbital methods. Furthermore, to elucidate the influence of these esters in vivo, we injected them into male mice and observed the change in the expression of PPARα-related enzymes. The comparison between the calculated and observed results indicates that the change in the expression has a correlation with the size of energy gaps between highest occupied and lowest unoccupied molecular orbitals of the complexes with mouse PPARα and esters.

1. Introduction

Peroxisome is an intracellular organelle and activates many enzymes to cause fatty acid β-oxidation involved in the generation of hydrogen peroxide (H_2O_2) [1,2]. Peroxisome proliferator-activated receptors (PPARs), which belong to the superfamily of steroid/nuclear receptors, regulate not only peroxisome proliferation but also many enzymes involved in peroxisome as well as mitochondria [3]. Accordingly, PPARs have various physiological functions such as lipid and glucose metabolism [3], inflammation [4] and fibrosis [5] in living organisms. Recent biomedical studies demonstrated that PPARs also participate in many disorders such as diabetes [6], cancer [7] and inflammatory disease [4].

The physiological functions of PPARs are controlled by many types of ligand molecules. It has been reported that PPARα, a subtype of the PPAR family, interacts not only with anti-hyperlipidemic agents but also with many chemicals such as the di-(2-ethylhexyl) phthalate used as a plasticizer [8]. However, there are only some structures of the ligand bound PPARα determined by experiments. Although various molecules bind to PPARα, their binding structures have not been clarified experimentally. To predict the effect of these ligand bindings on the function of PPARα, it is important to clarify the binding affinity of these ligand molecules to PPARα.

In the present study, we first investigated stable structures and their electronic properties for phthalate esters (DEP: diethyl phthalate; DBP: di-*n*-butyl phthalate; BBP: butylbenzyl phthalate; DCP: dicyclohexyl phthalate; DEHP: di-(2-ethylhexyl) phthalate), and an adipate ester (DEHA: di-(2-ethylhexyl) adipate), using ab initio molecular orbital (MO) calculations. These optimized structures of esters were docked to the ligand binding domain of PPARα to investigate the stable structures and electronic properties for the complexes of PPARα with these esters by molecular simulations based on molecular mechanics (MM) and MO methods. In addition, we conducted physiological experiments for SV/129 male mice to elucidate the influence of the ligand-injections on PPARα activity. These physiological experiments verified that there is a correlative relationship between the

* Corresponding author. Tel.: +81 532 44 6875; fax: +81 532 44 6875.
E-mail address: kurita@cochem2.tutkie.tut.ac.jp (N. Kurita).

1093-3263/$ – see front matter © 2008 Elsevier Inc. All rights reserved.
doi:10.1016/j.jmgm.2008.02.003

Table 1
Sequences of amino acids of human and mouse PPARα

(a) Human PPARα

	1	11	21	31	41
1	MVDTESPLCP	LSPLEAGDLE	SPLSEEFLQE	MGNIQEISQS	IGEDSSGSFG
51	FTEYQYLGSC	PGSDGSVITD	TLSPASSPSS	VTYPVVPGSV	DESPSGALNI
101	ECRICGDKAS	GYHYGVHACE	GCKGFFRRTI	RLKLVYDKCD	RSCKIQKKNR
151	NKCQYCRFHK	CLSVGMSHNA	IRFGRMPRSE	KAKLKAEILT	CEHDIEDSET
201	ADLKSLAKRI	YEAYLKNFNM	NKVKARVILS	GKASNNPPFV	IHDMETLCMA
251	EKTLVAKLVA	NGIQNKEAEV	RIFHCCQCTS	VETVTELTEF	AKAIPGFANL
301	DLNDQVTLLK	YGVYEAIFAM	LSSVMNKDGM	LVAYGNGFIT	REFLKSLRKP
351	FCDIMEPKFD	FAMKFNALEL	DDSDISLFVA	AIICCGDRPG	LLNVGHIEKM
401	QEGIVHVLRL	HLQSNHPDDI	FLFPKLLQKM	ADLRQLVTEH	AQLVQIIKKT
451	ESDAALHPLL	QEIYRDMY			

(b) Mouse PPARα

	1	11	21	31	41
1	MVDTESPICP	LSPLEADDLE	SPLSEEFLQE	MGNIQEISQS	IGEESSGSFG
51	FADYQYLGSC	PGSEGSVITD	TLSPASSPSS	VSCPVIPAST	DESPSSALNI
101	ECRICGDKAS	GYHYGVHACE	GCKGFFRRTI	RLKLVYDKCD	RSCKIQKKNR
151	NKCQYCRFHK	CLSVGMSHNA	IRFGRMPRSE	KAKLKAEILT	CEHDLKDSET
201	ADLKSLGKRI	HEAYLKNFNM	NKVKARVILA	GKTSNNPPFV	IHDMETLCMA
251	EKTLVAKIVA	NGVEDKEAEV	RFFHCCQCMS	VETVTELTEF	AKAIPGFANL
301	DLNDQVTLLK	YGVYEAIFTM	LSSLMNKDGM	LIAYGNGFIT	REFLKNLRKP
351	FCDIMEPKFD	FAMKFNALEL	DDSDISLFVA	AIICCGDRPG	LLNIGYIEKL
401	QEGIVHVLKL	HLQSNHPDDT	FLFPKLLQKM	VDLRQLVTEH	AQLVQVIKKT
451	ESDAALHPLL	QEIYRDMY			

DNA and ligand binding domains are colored in red and blue, respectively. The different amino acids between human and mouse PPARα are marked by yellow.

expression of PPARα-related enzymes and the molecular weight or hydrophobicity of the injected ligand molecules. From the comparison between the present calculated and experimental results, we attempted to make clear the relations between the change in the expression of PPARα-related enzymes induced by the ligand injection and the electronic properties of the complexes with PPARα and ligand molecules.

2. Details of molecular simulations

2.1. Construction of PPARα structures for human and mouse

Initial structures of the ligand binding domain (LBD) for human PPARα (hPPARα) and mouse PPARα (mPPARα) were constructed based on the X-ray crystal structure of the complex with hPPARα and GW409544 ligand [9], whose PDB code is 1K7L. As for the crystal structure of hPPARα, the 1I7G [10] structure is also registered in PDB. In the present study, we used the 1K7L structure, because there are some missing amino acids in the 1I7G structure. The 1K7L structure contains a tetramer of the LBD of hPPARα (hPPARα-LBD). We thus extracted a monomer from the tetramer by using the molecular modeling software HyperChem [11]. The 1K7L structure also contains crystallization water molecules, some of which can contribute to the specific binding between the amino acids of hPPARα and ligand. Accordingly, we considered the 74 water molecules within 8.0 Å distance from the monomer of the hPPARα-LBD in the present molecular simulations. This PDB X-ray structure of the hPPARα-LBD has no hydrogen atoms, so that we added hydrogen atoms by using HyperChem and optimized their positions with fixing the other part by using the classical MM method based on the AMBER [12] force field. The optimized structure was used as an initial structure of the complex with hPPARα-LBD and GW409544.

To construct the structure of mPPARα-LBD, we checked the difference in the sequence of amino acids between hPPARα and mPPARα. The 1K7L PDB structure of hPPARα-LBD contains 267 amino acids between 202nd and 468th. As shown in Table 1, among these 267 amino acids, 21 amino acids are different between hPPARα and mPPARα [13], so that we replaced these 21 amino acids in hPPARα by the amino acids corresponding to mPPARα and optimized the structures of the replaced amino acids by the classical MM method with AMBER force field. In this procedure, in order to prevent bending the side chains of the replaced amino acids and binding them to the main chain, we replaced one amino acid and optimized its structure with fixing the other part. This procedure was repeated sequentially for the 21 amino acids to obtain the initial structure of the complex with mPPARα-LBD and GW409544.

2.2. Structure optimizations and MO calculations for ester ligands

In the present physiological experiment, we injected five types of plasticizing phthalate esters (DEP, DBP, BBP, DCP and DEHP) and an adipate ester DEHA into the mice to observe their effect on the expression of the PPARα-related enzymes. The chemical structures of these esters are shown in Fig. 1. In order to predict the specific interactions between PPARα-LBD and these esters by molecular simulations, it is important to obtain realistic structures of these esters binding to PPARα-LBD and to dock them accurately into the binding pocket of PPARα-LBD. As shown in Fig. 1, the di-forms of these esters are considered to be hydrolyzed into the mono-forms in living organisms [14–19], and their anions are expected to bind to the binding pocket of PPARα-LBD with the carboxyl COO^- part.

In the present study, we considered that the ligand structures in the binding pocket of PPARα-LBD are significantly different from those in vacuum and constructed the initial structures of the six types of esters based on the experimentally obtained structure [9] of GW409544 ligand bound to hPPARα-LBD. Since the COO^- part of GW409544 contributes to the binding between GW409544 and hPPARα-LBD, we constructed the initial structures of the esters on the assumption that their COO^- parts overlap the COO^- part of GW409544. These structures can be inserted into the binding pocket of hPPARα-LBD without a large steric constraint between the esters and the side chains of the amino acids existing in the binding pocket of hPPARα-LBD.

In fact, we first constructed the initial structures for the mono-forms of the six types of esters based on the GW409544 structure bound to hPPARα-LBD (PDB code: 1K7L) and optimized them by

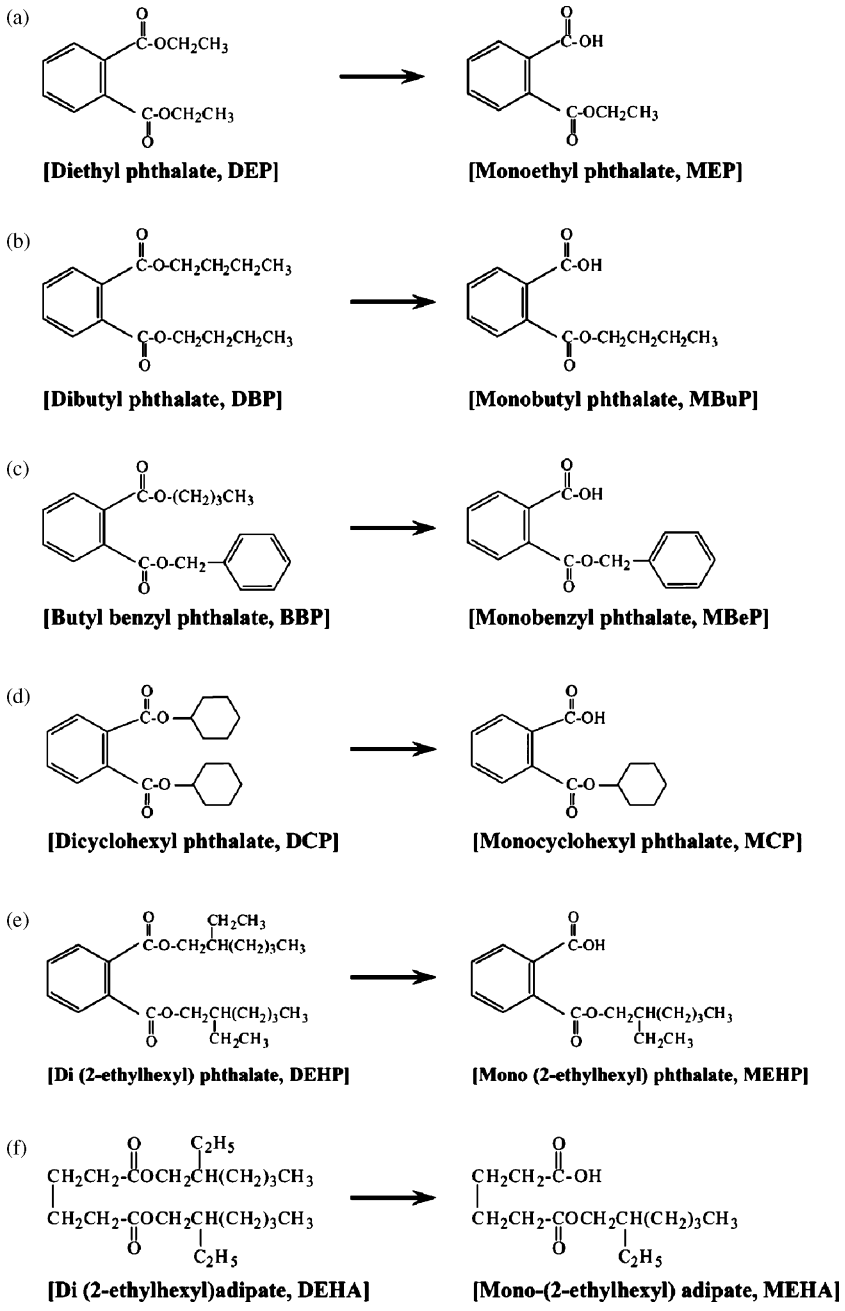

Fig. 1. Chemical structures of the di- and mono-forms of phthalate and adipate esters used in the present physiological experiments, and their hydrolyzations into the mono-forms in living organisms: (a) from di-ethyl phthalate (DEP) to mono-ethyl phthalate (MEP); (b) from di-butyl phthalate (DBP) to mono-butyl phthalate (MBuP); (c) from butyl benzyl phthalate (BBP) to mono-benzyl phthalate (MBeP); (d) from di-cyclohexyl phthalate (DCP) to mono-cyclohexyl phthalate (MCP); (e) from di-(2-ethylhexyl) phthalate (DEHP) to mono-(2-ethylhexyl) phthalate (MEHP); (f) from di-(2-ethylhexyl) adipate (DEHA) to mono-(2-ethylhexyl) adipate (MEHA).

the semiempirical MO method (PM3 method [20]) implemented in the semiempirical MO program package MOPAC [21]. These structures were furthermore optimized by using the ab initio MO program Gaussian03 [22] to obtain more accurate structures of the esters similar to the GW409544 bound to hPPARα-LBD. In these optimizations, we used the second-order Moller-Plesset (MP2) method [23] along with the 6–31G** basis set (standard split-valence 6–31G basis sets augmented by a set of d- and p-polarization functions assigned to heavy atoms and hydrogen atom, respectively). Finally, to predict the strength of electrostatic interaction between hPPARα and the six types of esters, their charge distributions around the COO^- part were analyzed by the Merz–Kollman's method [24].

In the classical MM calculations, parameters in the force field are indispensable. The AMBER force field [12] has parameters for all amino acids of proteins. However, there is no parameter provided for ligand molecules such as GW409544, phthalate esters and an adipate ester shown in Fig. 1. We thus performed the restrained electrostatic potential (RESP) calculations [25] for the optimized structures by the MP2/6–31G** method. Based on the RESP results, atomic charges for each atom of these ligand molecules were determined, and the electric charge parameters in the AMBER force field were produced. Furthermore, the AMBER parameters for van der Waals interactions, the bond length between atoms, torsion angles and dihedral angles were selected from the prepared AMBER parameters.

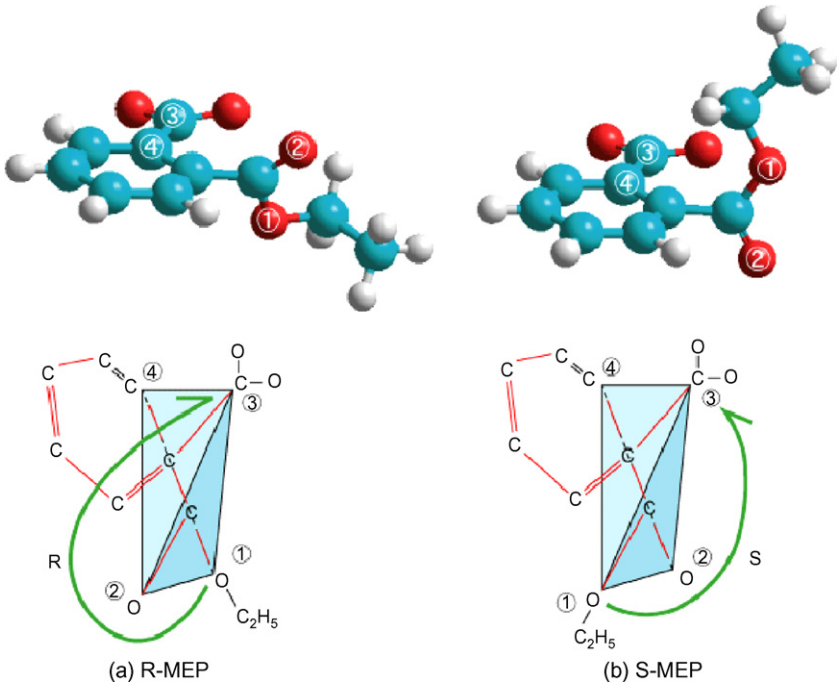

Fig. 2. Definitions of ***R***- and ***S***-forms for the mono-form of MEP.

2.3. Structure optimizations for the complexes with PPARα-LBD and ester ligands

The initial structures of the complexes with hPPARα-LBD and the six types of esters were constructed based on the X-ray crystal structure of the hPPARα-LBD + GW409544 complex (PDB code is 1K7L). By using HyperChem software [11], the GW409544 part was replaced by the six types of mono-form esters, whose structures were optimized in a vacuum by the MP2/6–31G** method of the Gaussian03 program [22]. Since the size of the mono-forms is smaller than that of GW409544, some substituted groups of the mono-forms can rotate freely, so that some rotational isomers can be inserted into the binding pocket of hPPARα-LBD. In the present study, we considered two kinds of rotational isomers and docked them into the binding pocket of hPPARα-LBD by using HyperChem. For example, the two isomers of MEP were defined as *R*- and *S*-form structures in accordance with the concept of facial chirality, as shown in Fig. 2. As for the large-sized adipate mono-ester (MEHA), only the *S*-form can be inserted into the binding pocket of hPPARα-LBD, because of the large steric constraint between the *R*-form MEHA and hPPARα-LBD. In replacing GW409544 by the mono-forms of esters, the

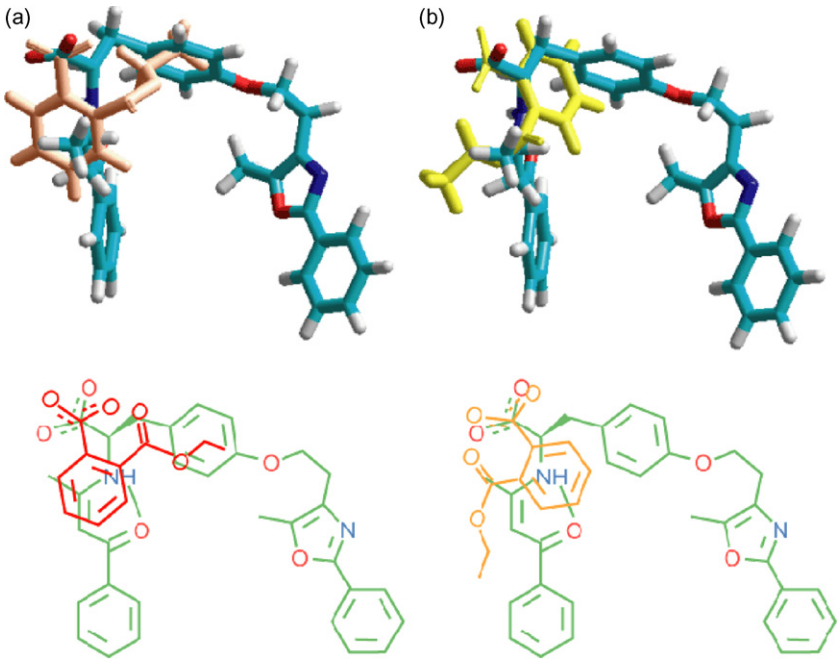

Fig. 3. Orientations of the mono-form MEP in the ligand-binding pocket of hPPARα-LBD: (a) ***R***-MEP is superposed on the phenylpropionic acid part of GW409544; (b) ***S***-MEP is superposed on the other part of GW409544.

mono-forms were spatially situated as the COO^- part of the ester overlaps the COO^- part of GW409544, as shown in Fig. 3, because the COO^- part is expected to mainly contribute to the binding between these esters and hPPARα-LBD. For example, as shown in Fig. 3(a), the *R*-form MEP was superposed on the phenylpropionic acid part of GW409544, while the *S*-form MEP was superposed on the opposite side of the phenylpropanoic acid part, as shown in Fig. 3(b).

The constructed initial structures of the complexes for hPPARα-LBD + mono-form esters with crystal water molecules were optimized by the classical MM method based on our produced AMBER force field. The MM calculation program TINKER [26] was used for these optimizations, in which the steepest descent method was used. The effect of solvation was considered with the continuum solvent approximation by Still [27]. The threshold value of the energy-gradient for the convergence of optimization was set to be 0.01 kcal/(mol Å). The structures of the complexes with mPPARα-LBD and ligands were optimized in the same way as for the hPPARα-LBD complexes.

2.4. MO calculations for optimized structures of PPARα-LBD + ligands

In order to elucidate the affinity between PPARα-LBD and the ligand molecules such as GW409544 and esters, we investigated the binding energies between PPARα-LBD and ligands by using the semiempirical MO method (PM3 method [20]). Since the electrostatic interaction between PPARα-LBD and ligands is overestimated by the MO calculation in vacuum, the MO calculations were performed in water approximated by the continuum solvation model COSMO [28]. Note that the experimental structure of the hPPARα-LBD + GW409544 complex has some water molecules around the GW409544 binding site, and that these water molecules contribute to the interactions between GW409544 and the amino acids of hPPARα-LBD. Therefore, in the present study, we considered these water molecules explicitly in the MO calculations. The binding energy between hPPARα-LBD and ligands mediated by these water molecules was estimated from the difference between the heat of formation for the complex of hPPARα-LBD + ligand + water molecules and the sum of each heat of formation for hPPARα-LBD, ligand, and water molecules. From the comparison of the obtained binding energies, it was elucidated which ligand molecule has large affinity to hPPARα-LBD.

We furthermore analyzed the energy levels and spatial distributions of HOMO (highest occupied MO) and LUMO (lowest unoccupied MO) to elucidate how the chemical reactivity and the reactive part of hPPARα-LBD are affected by the binding of GW409544 as well as the six types of ester ligands. The same analysis was performed for the complexes with mPPARα-LBD and ligands.

3. Physiological experiment on the effect of ligand injection on PPARα activation

The present physiological study was conducted according to the Guidelines for Animal Experiments of the Shinshu University Animal Center. SV/129 male mice with 16 weeks age were used, and they were housed in a clean room under controlled temperature, humidity, light and darkness. Commercial solid feed and water were given freely. The 5.0 mmol/kg of each phthalate esters (DEP, DBP, BBP, DCP and DEHP) and an adipate ester (DEHA) were injected into the mice by using gavage once a day for 14 days. In general, peroxisome proliferators induce the activation of PPARα-target genes in the 2 weeks exposure [29,30]. In the present study, these injected mice were dissected after 16 h of the last treatment, and their livers were removed to be stored at −80 °C.

Peroxisome proliferation and fatty acid β-oxidation enzymes are strongly controlled by PPARα. Western blot analysis was conducted to check the induction of hepatic PPARα-related enzymes in the peroxisome and mitochondria enzymes. Liver homogenates adjusted to 10 μg protein were subjected to 10% SDS-PAGE and transferred to nitrocellulose membranes. After blocking with 3% skim milk, each membrane was incubated with the primary antibody, followed by incubation with alkaline phosphatase-conjugated goat anti-rabbit IgG (Jackson Immuno Research, West Grove, PA) and color development by 1-step TM NBT/BCIP (Pierce, USA). The primary polyclonal antibodies were prepared using purified peroxisomal thiolase (PT) [31], bifunctional protein (PH) [32], mitochondrial acyl-CoA dehydrogenase (VLCAD) [33], trifunctional protein α subunit (TPα) and 3-ketoacyl-CoA thiolase (TPβ) [34]. These antibodies have already been used in the previous studies [29,30]. Each band was quantified by densitometry, using the Lane & Spot Analyzer version 5.0 (ATTO Corporation, Tokyo, Japan). Comparisons were made using the one-way analysis of variance (ANOVA). A probability level of <0.05 was used as the criterion of significance.

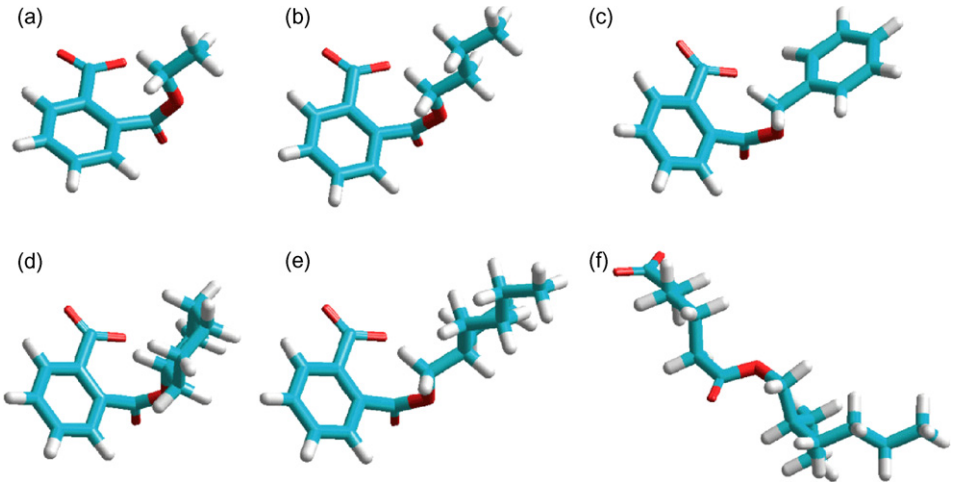

Fig. 4. Optimized structures of the mono-forms of the six types of esters by the MP2/6-31G** method: (a) MEP; (b) MBuP; (c) MBeP; (d) MCP; (e) MEHP and (f) MEHA. Their atomic coordinates are given as supplementary information.

4. Results and discussion

4.1. Optimized structures and electronic properties for mono-forms of esters

In order to accurately predict the interaction between PPARα and ligands, it is important to obtain the electronic properties of ligands, whose structures are similar to those bound to the ligand-binding pocket of PPARα. We thus constructed the initial structures for the mono-form esters based on the GW409544 structure bound to hPPARα-LBD (PDB code: 1K7L [9]) and optimized them by the MP2/6–31G** method to obtain stable structures similar to the GW409544 bound to hPPARα-LBD. The optimized structures and their electronic properties are compared in Fig. 4 and Table 2, respectively. The energy levels of HOMO and LUMO were obtained at the Hartree–Fock level of theory. The atomic coordinates of these structures in Fig. 4 are given as supplementary information.

MEP (Fig. 4(a)) and MBuP (Fig. 4(b)) have a short side chain, so that it is expected that they are easily inserted into the ligand-binding pocket of PPARα-LBD and can rotate in the pocket. On the other hand, because MBeP (Fig. 4(c)) and MCP (Fig. 4(d)) have a sterically bulky side chain with a ring structure, they can not rotate in the pocket. Although MEHP (Fig. 4(e)) and MEHA (Fig. 4(f)) have a long and bulky side chain with an ethylhexyl group, both ligands can be inserted into the pocket, because MEHA has no ring structure. In addition, MEHA has a straight chain structure similar to the phenylpropanoic acid part of GW409544 (Fig. 6), indicating the possibility that the interaction between MEHA and PPARα-LBD is similar to that between GW409544 and PPARα-LBD.

As shown in Table 2, the energy levels of HOMO and LUMO for the five types of the mono-form phthalate esters are similar to one another, while those for the adipate ester MEHA are about 1 eV higher than those for the phthalate esters. On the other hand, the energy gap between HOMO and LUMO is similar for all the six types of esters. Note that the atomic charges of the oxygen atoms of COO^- part are remarkably different among the six esters. The values for MBuP, MEHA and MBeP are negatively larger than those for the other esters, indicating that MBuP, MEHA and MBeP can bind stronger to the binding pocket of PPARα-LBD, because the COO^- part is the main part contributing to the binding between GW409544 and PPARα-LBD. However, these atomic charges of COO^- part can not explain the experimentally obtained trend for the activation of PPARα-related enzyme expression induced by the injection of esters, as will be shown in Section 4.6.

Table 2
Total energies (Hartree), energy levels (eV) of HOMO and LUMO, their energy gaps (eV), and averaged Merz–Kollman's atomic charges of two oxygen atoms of the COO^- part for the mono-forms of ester molecules optimized by MP2/6–31G**

Molecules	Total energy	HOMO	LUMO	H–L Gap	Charge of O atom
MEP	−685.4863	−5.700	6.559	12.259	−0.635
MBuP	−763.8506	−5.715	6.545	12.260	−0.729
MBeP	−876.6411	−5.866	6.323	12.189	−0.714
MCP	−841.0441	−5.776	6.454	12.230	−0.628
MEHP	−920.5818	−5.798	6.454	12.252	−0.662
MEHA	−846.9555	−4.795	7.288	12.083	−0.728

4.2. Optimized structures of human and mouse PPARα-LBDs + GW409544 complexes

To check the accuracy of the optimization method based on the AMBER [12] force field and the continuum solvation model by Still [27], we first compared the optimized structure of the hPPARα-LBD + GW409544 complex with its X-ray crystal structure [9]. The root mean square distance (RMSD) between the two structures are 1.53 Å for all the atoms and 1.30 Å for only Cα atoms. Therefore, the optimized structure of hPPARα-LBD + GW409544 is found to be comparable to the X-ray crystal structure. The two structures are superimposed in Fig. 5. There is no remarkable difference between them in the ordered domains having α-helix or β-sheet structure, while the flexible parts with loop structure between the domains have a different structure in the optimized and experimental ones as shown in Fig. 5(a). In addition, the close-up view of GW409544 (Fig. 5(b)) indicates that the position and conformation of GW409544 in the hPPARα-LBD obtained by the present method is comparable to the experimental one.

The specific interaction between hPPARα-LBD and GW409544 was elucidated in the X-ray crystal structure [9]. As shown in Fig. 6,

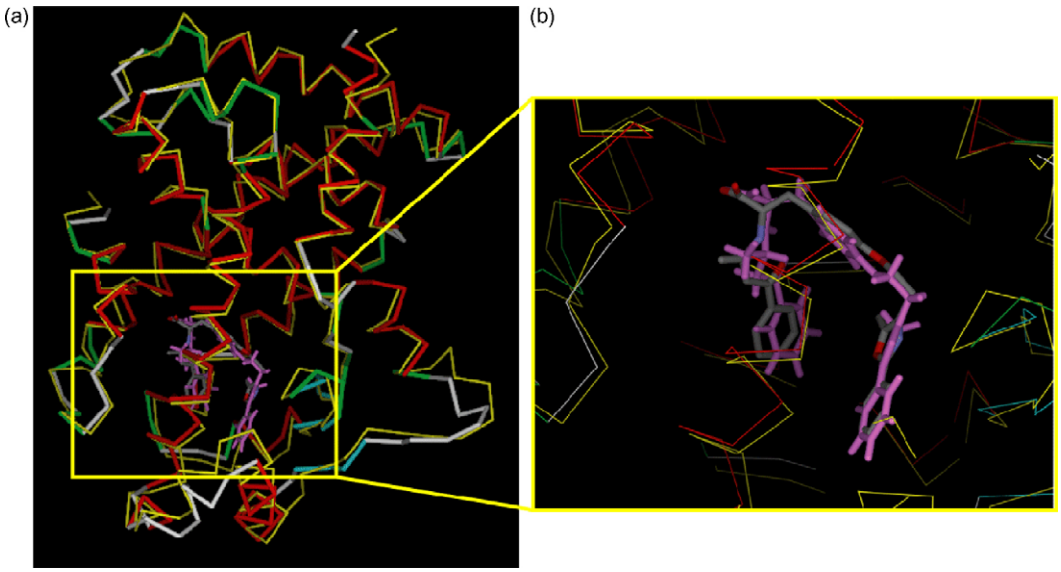

Fig. 5. Comparison of the optimized and X-ray crystal structures for the complex with hPPARα-LBD and GW409544: (a) positions of Cα atoms of hPPARα-LBD and GW409544, in which helices, β sheets, turns and coils of the X-ray structure are depicted in red, cyan, green and white, respectively, while the optimized structure is in yellow; (b) close-up view around GW409544, in which the X-ray and optimized structures of GW409544 are colored by atom-type and purple, respectively.

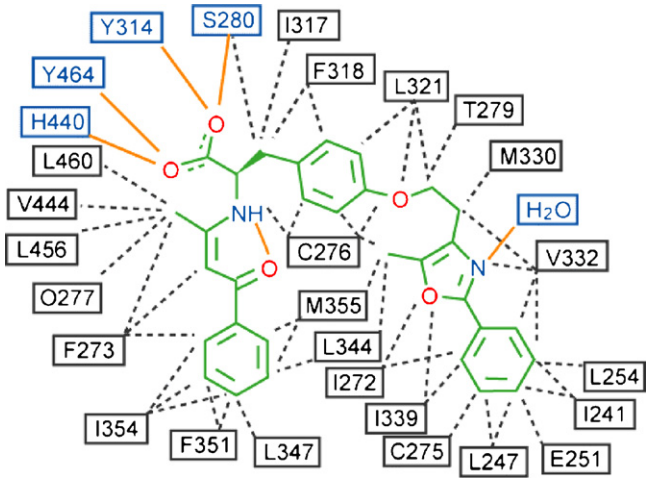

Fig. 6. Amino acids of hPPARα-LBD interacting with GW409544 in the X-ray crystal structure [9]. The hydrogen-bonding and hydrophobic interactions are indicated by the full and broken lines, respectively. The COO^- part of GW409544 mainly contributes to the hydrogen-bonding interactions between hPPARα-LBD and GW409544.

there are 28 amino acids of hPPARα-LBD considered to be important in the interaction to GW409544. To confirm that the present optimization method can reproduce this specific interaction, we checked the amino acids existing within 4.0 Å distance from GW409544 in both the X-ray and our optimized structures. As shown in the second column of Table 3, among the 28 amino acids shown in Fig. 6, the 25 amino acids except for the 3 amino acids (I317, I241, V444) exist within 4.0 Å distance from GW409544 in the X-ray crystal structure. On the other hand, in the optimized structure, the 24 amino acids except for the 4 amino acids (I241, L456, V444, L460) among the 28 amino acids exist within 4.0 Å distance. Table 3 clarifies that the X-ray crystal structure and the optimized one of hPPARα-LBD around GW49544 are in agreement with each other except for the three amino acids (I317, L456, L460).

In order to reveal the difference in structure between human and mouse PPARα-LBDs and predict their specific interactions with various ligands, we optimized the structure of the mPPARα-LBD + GW409544 complex. Although there are 21 amino acids

Table 3
Comparison of specific interactions between PPARα-LBD and GW409544 in the X-ray crystal structure [9] and the optimized structure

Amino acids or H_2O	Human PPARα		Mouse PPARα	
	Crystal structure	Optimized structure	Different amino acids	Optimized structure
H440	Y	Y		Y
Y464	Y	Y		Y
Y314	Y	Y		Y
S280	Y	Y		Y
I317	–	Y		–
F318	Y	Y		Y
L321	Y	Y		Y
T279	Y	Y	M279	Y
M330	Y	Y		Y
H_2O	–	–		Y
V332	Y	Y	I332	Y
L254	Y	Y		Y
I241	–	–		–
E251	Y	Y		Y
L247	Y	Y		–
C275	Y	Y		Y
I339	Y	Y		–
I272	Y	Y	F272	Y
L344	Y	Y		Y
M355	Y	Y		Y
C276	Y	Y		Y
L347	Y	Y		Y
F351	Y	Y		Y
I354	Y	Y		Y
F273	Y	Y		Y
Q277	Y	Y		Y
L456	Y	–		Y
V444	–	–		Y
L460	Y	–		Y

The amino acids of PPARα-LBD existing within 4.0 Å distance from GW409544 are marked with Y.

difference between the hPPARα-LBD and mPPARα-LBD, the RMSD value for Cα atoms between the optimized structures of hPPARα-LBD and mPPARα-LBD was evaluated to be 1.08 Å, indicating that the effect of the difference in amino acids on the structure of the human and mouse PPARα-LBDs is not so large.

We furthermore investigated the amino acids participating to the interactions between mPPARα-LBD and GW409544 to make clear the difference in specific interactions between the human and

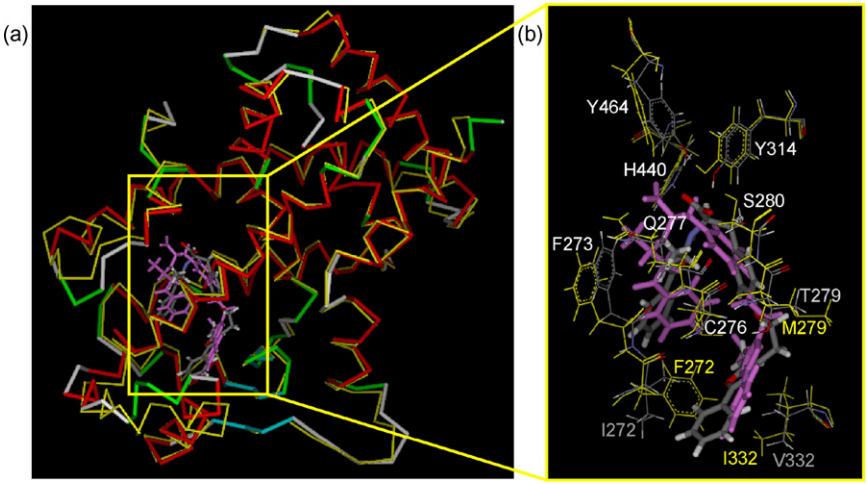

Fig. 7. Comparison of the optimized structures for the complexes with human and mouse PPARα-LBDs and GW409544: (a) positions of Cα atoms of PPARα-LBDs and GW409544, in which helices, β sheets, turns and coils of hPPARα-LBD are depicted in red, cyan, green and white, respectively, while all parts of mPPARα-LBD are in yellow; (b) close-up view around GW409544, in which GW409544 in hPPARα-LBD is colored by atom-type, while GW409544 in mPPARα-LBD is depicted in purple. Amino acids existing around GW409544 are indicated, in which the amino acids in mPPARα-LBD are in yellow.

mouse PPARα-LBDs. The amino acids existing within 4.0 Å distance from GW409544 in the mPPARα-LBD + GW409544 are listed in Table 3. The comparison between the human and mouse PPARα-LBDs indicates that there are six amino acids (I317, L247, I339, L456, V444, L460) differences between them. In addition, as shown in Fig. 7, the conformation and position of GW409544 in the ligand-binding pockets of the human and mouse PPARα-LBDs are remarkably different each other. In the hPPARα-LBD + GW409544 complex, the COO^- part of GW409544 binds to the S280, Y314, H440, Y464 amino acids of LBD, whereas the position and direction of the COO^- part in mPPARα-LBD are largely different from those in hPPARα-LBD.

In the experimental study [9], it was concluded that the Y464 and Y314 amino acids are important for the ligand binding of hPPARα-LBD. This result is consistent with our calculated result for the hPPARα-LBD + GW409544 complex. In addition, the calculated result for mPPARα-LBD elucidates that the position of Y464 side-chain in mPPARα-LBD shifts away from the COO^- part of GW409544, as shown in Fig. 7(b). It is thus proposed that the difference in position of Y464 amino acid in the human and mouse PPARα-LBDs is one of the reasons for the difference in ligand binding affinity between these PPARα-LBDs.

In the previous molecular simulations [35] for the complexes with PPARα-LBDs and 2-ethylphenylpropanoic acid derivative (KCL), it was suggested that the difference of the 272nd amino acid (I and F) between the human and mouse PPARα-LBDs affects the binding position of the KCL ligand. The I272 amino acid of hPPARα-LBD has no ring structure, while the F272 amino acid of mPPARα-LBD has a bulky side chain with a benzyl group. It was thus proposed [35] that the steric hindrance between the bulky benzyl group of F272 and the tail of GW409544 causes a large shift of GW409544 in mPPARα-LBD. In the present molecular simulations, we obtained the stable structures of the complexes with these PPARα-LBDs and GW409544 (Fig. 7) and elucidated that the tail part of GW409544 in mPPARα-LBD is affected by the side chain of F272 to change the conformation widely, as shown in Fig. 7(b). As the result, GW409544 shifts upwards in mPPARα-LBD compared with GW409544 in hPPARα-LBD.

4.3. Optimized structures of human and mouse PPARα-LBDs + esters complexes

To elucidate the difference in ligand-binding affinity of human and mouse PPARα-LBDs, the difference in these structures bound by the six types of esters were analyzed. In Fig. 8, the positions of Cα atoms for these PPARα-LBDs as well as the ester ligands are superposed. As a whole, the Cα positions are not so largely different between these ligand-bound PPARα-LBDs. However, the Cα positions of the lower part in Fig. 8, which is composed by loop and turn domains, are different from each other. Since this part

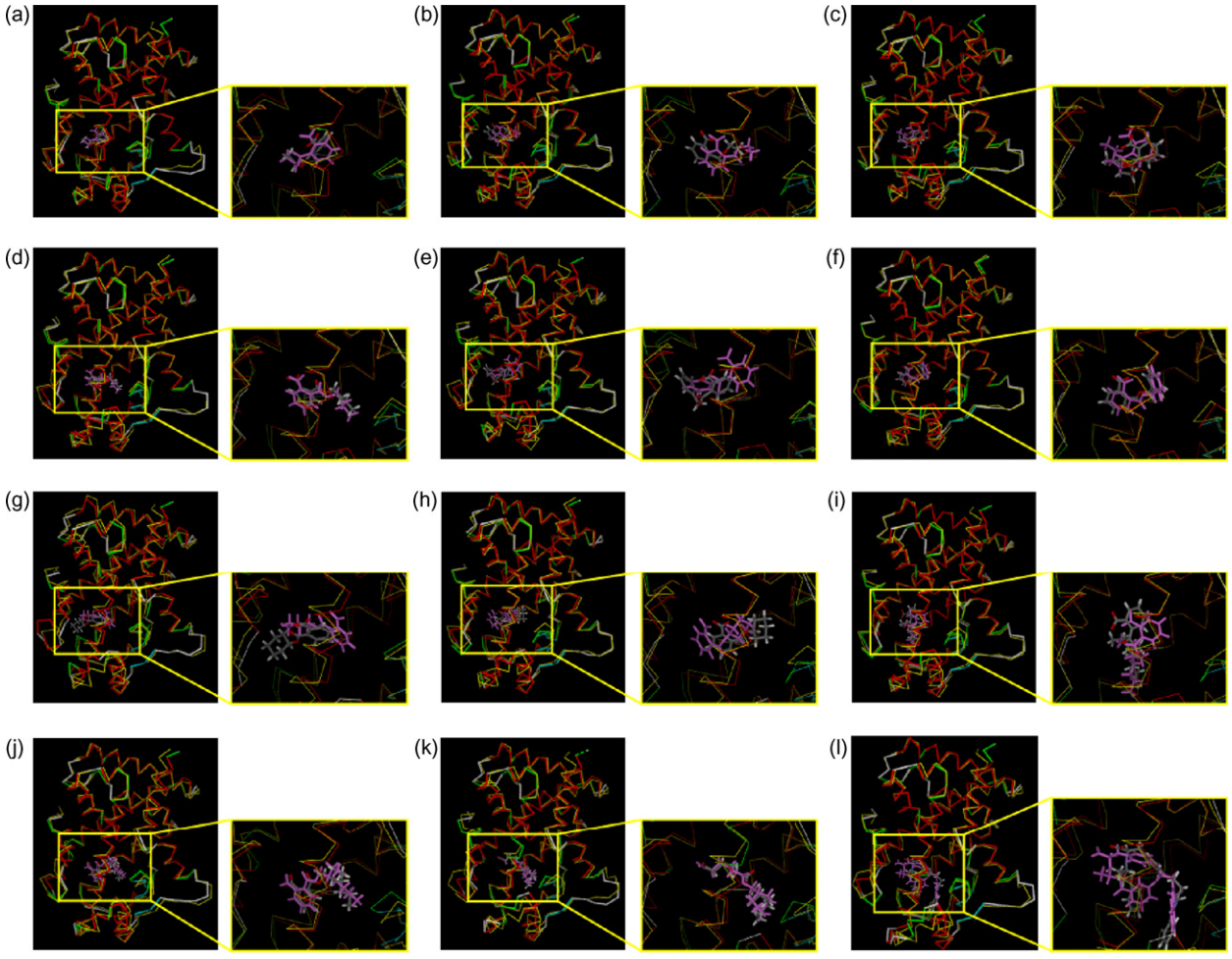

Fig. 8. Comparison of the optimized structures for the complexes of human and mouse PPAR**α**-LBDs + ester and GW409544 ligands: (a) ***S***-MEP; (b) ***R***-MEP; (c) ***S***-MBuP; (d) ***R***-MBuP; (e) ***S***-MBeP; (f) ***R***-MBeP; (g) ***S***-MCP; (h) ***R***-MCP; (i) ***S***-MEHP; (j) ***R***-MEHP; (k) ***S***-MEHA and (l) GW409544. In the left-hand figures, helices, **β** sheets, turns and coils of hPPAR**α**-LBD are depicted in red, cyan, green, and white, respectively, while all parts of mPPAR**α**-LBD are in yellow. The right-hand figures are close-up views around ligands, in which the structures of ligands in hPPAR**α**-LBD are colored by atom-type, while those in mPPAR**α**-LBD are in purple.

Table 4
Comparison of structures and electronic properties for the complexes of (a) human and (b) mouse PPARα-LBDs + GW409544 or S-form ester ligands: (i) RMSD values (Å) of Cα atoms between PPARα-LBD + GW409544 and PPARα-LBD + ester complexes; (ii) hydrogen bond distances (Å) between COO^- of ligand and PPARα-LBD, the values in parentheses are hydrogen bond distances between the other parts of COO^- and PPARα-LBD; (iii) total numbers of hydrogen bonds between ligand and PPARα-LBD, (iv) heat of formations and binding energies (B.E.) (kcal/mol) for the complexes of PPARα-LBD and ligand, (v) energy levels (eV) and spatial distributions of HOMO and LUMO for the complexes of PPARα-LBD and ligand, and the energy gaps (eV) between HOMO and LUMO

(a) Human PPARα + ligands							
Ligand	GW409544	*S*-MEP	*S*-MBuP	*S*-MBeP	*S*-MCP	*S*-MEHP	*S*-MEHA
(i) RMSD							
	–	0.92	0.84	1.03	1.32	0.72	0.85
(ii) H-bond lengths							
H440	1.77	–	–	–	–	–	1.75
Y464	1.90	–	–	1.98	1.82	1.73	1.89
Y314	1.78, 2.73	1.77	1.73	1.73, 2.79	1.75	–	1.76
S280	1.59	1.68	1.67	1.67	1.70	–	1.69
C276	–	–	–	–	–	–	2.29
Q277	–	–	–	–	–	–	–
(iii) Number of H-bonds							
	5	2	2	4	3	1	4 (1)
(iv) H.O.F and B.E.							
PPARα + ligand + H_2Os	−19188.20	−19191.60	−19201.82	−19163–58	−19215.70	−19241.43	−19304.08
PPARα	−14720.05	−14655.56	−14666.09	−14670.39	−14667.59	−14699.26	−14687.12
H_2Os	−4278.73	−4278.68	−4277.01	−4277.44	−4278.73	−4276.93	−4277.97
Ligand	−168.37	−226.92	−232.73	−188.69	−237.52	−251.91	−298.69
B.E.	−21.05	−30.44	−25.99	−27.06	−31.87	−13.32	−40.30
(v) Energy levels and spatial distributions of HOMO and LUMO							
HOMO	−8.59	−8.53	−8.50	−8.56	−8.71	−8.56	−8.57
	M467	E251	E286	E251	Y214	E251	E251
LUMO	−2.19	3.16	−3.01	−2.59	−2.63	−3.11	−2.29
	H440	H440	H440	H440	H440	H440	H440
Gap	6.40	5.37	5.50	5.98	6.09	5.45	6.28
(b) Mouse PPARα + ligands							
Ligand	GW409544	*S*-MEP	*S*-MBuP	*S*-MBeP	*S*-MCP	*S*-MEHP	*S*-MEHA
(i) RMSD							
	–	1.11	1.17	1.07	1.08	1.14	0.91
(ii) H-bond lengths							
H440	1.75	–	1.96	1.80	–	1.88	1.72
Y464	1.75	–	–	–	–	–	1.95
Y314	–	–	–	–	–	–	–
S280	–	1.68	1.74	1.84, (2.70)	1.69	1.91	1.67
C276	–	–	–	–	–	–	–
Q277	1.85	–	–	–	–	–	–
(iii) Number of H-bonds							
	3	1	2	2 (1)	1	2	3
(iv) H.O.F and B.E.							
PPARα + ligand + H_2Os	−19433.76	−19535.20	−19507.80	−19466.15	−19499.79	−19545.29	−19594.38
PPARα	−14971.03	−15018.66	−14980.95	−14994.42	−14982.38	−14993.13	−14976.13
H_2Os	−4276.38	−4274.06	−4273.21	−4276.84	−4284.36	−4273.42	−4275.81
Ligand	−171.44	−225.04	−232.78	−189.07	−240.21	−249.40	−307.35
B.E.	−14.91	−17.44	−20.85	−5.82	−2.84	−29.33	−35.08
(v) Energy levels and spatial distributions of HOMO and LUMO							
HOMO	−8.06	−8.38	−8.40	−8.06	−8.22	−8.61	−8.28
	E264	Lignad	E264	E264	Ligand	M467	E264
LUMO	−3.10	−1.71	−1.64	−1.83	−2.73	−1.45	−2.33
	H440	H440	H440	Ligand	H440	H440	H440
Gap	4.97	6.68	6.75	6.23	5.49	7.16	5.94

exists near the entrance of the ligand-binding pocket, the difference in structure of this part may cause the difference in the mechanism of ligand insertion into the pocket of PPARα-LBD, resulting in the difference in ligand-binding affinity between the human and mouse PPARα-LBDs. Molecular dynamics simulations are required for elucidating the mechanism of ligand insertion into these PPARα-LBDs.

As shown in Fig. 8(k) and (l), the binding modes of S-MEHA having no aromatic ring in the human and mouse PPARα-LBDs are almost the same as that of GW409544 in hPPARα-LBD. However, the hydrogen bonding structure between PPARα-LBD and S-MEHA/GW409544 is different for the human and mouse PPARα-LBDs, as shown in Table 4(ii). In the hPPARα-LBD + S-MEHA complex, four amino acids (Y314, H440, Y464 and S280) are hydrogen bonded to S-MEHA, while only three amino acids (H440, Y464 and S280) are bonded in the mPPARα-LBD + S-MEHA complex. As for the PPARα-LBD + GW409544 complexes, hPPARα-LBD has the same four hydrogen bonded amino acids as those in the hPPARα-LBD + S-MEHA, while mPPARα-LBD has only two (H440 and Y464) amino acids hydrogen bonding to GW409544. These differences in

Table 5
Comparison of structures and electronic properties for the complexes of (a) human and (b) mouse PPARα-LBDs + *R*-form ester ligands; the details are the same as in Table 4

Ligand	*R*-MEP	*R*-MBuP	*R*-MBeP	*R*-MCP	*R*-MEHP
(a) Human PPARα + ligands					
(i) RMSD					
	0.76	0.81	0.80	0.80	0.77
(ii) H-bond lengths					
H440	1.88	1.82	1.84	–	1.85
Y464	2.56	2.50	–	–	–
Y314	1.76, 2.61	1.70	1.80, 2.67	1.78, 2.49	1.85
S280	1.78	1.76	–	1.76	–
C276	–	–	1.92	2.44	–
Q277	–	–	–	–	–
(iii) Number of H-bonds					
	5	3 (1)	3 (1)	3 (1)	1 (1)
(iv) H.O.F and B.E.					
PPARα + ligand + H_2Os	−19228.90	−19230.90	−19201.71	−19238.18	−19222.42
PPARα	−14687.24	−14673.17	−14680.47	−14685.28	−14653.79
H_2Os	−4276.73	−4277.02	−4278.13	−4276.09	−4281.38
Ligand	−222.19	−238.37	−189.24	−236.16	−255.27
B.E.	−42.73	−42.35	−53.87	−40.66	−31.99
(v) Energy levels and spatial distributions of HOMO and LUMO					
HOMO	−8.52	−8.51	−8.53	−8.50	−8.63
	E251	E251	E251	E251	M467
LUMO	−2.59	−2.69	−2.37	−2.58	−2.08
	H440	H440	H440	H440	H440
Gap	5.93	5.82	6.16	5.92	6.55
(b) Mouse PPARα + ligands					
Ligand	*R*-MEP	*R*-MBuP	*R*-MBeP	*R*-MCP	*R*-MEHP
(i) RMSD					
	1.16	1.33	1.12	1.39	1.15
(ii) H-bond lengths					
H440	1.84	1.82	1.82	1.81	1.92
Y464	–	2.34	–	1.85	–
Y314	1.77, 2.54	1.68	1.74	1.78, 2.73	1.86
S280	1.71	1.75	–	–	–
C276	–	–	1.97	–	–
Q277	–	1.85	–	–	–
(iii) Number of H-bonds					
	4	4 (1)	2 (1)	4	1 (1)
(iv) H.O.F and B.E.					
PPARα + ligand + H_2Os	−19478.40	−19518.84	−19458.77	−19475.19	−19506.74
PPARα	−14943.52	−14963.35	−14979.37	−14948.18	−14958.01
H_2Os	−4276.89	−4276.37	−4277.75	−4276.67	−4276.67
Ligand	−226.99	−238.24	−189.72	−231.02	−254.85
B.E.	−31.00	−40.89	−11.93	−19.31	−17.13
(v) Energy levels and spatial distributions of HOMO and LUMO					
HOMO	−8.74	−8.60	−8.67	−8.76	−8.59
	M467	M467	M467	M467	M467
LUMO	−2.92	−2.51	−2.43	−2.53	−1.71
	H440	H440	H440	H440	H440
Gap	5.82	6.09	6.24	6.23	6.88

hydrogen bonding structure may cause a remarkable difference in binding energy between human and mouse PPARα-LBDs and ligand as shown in Tables 4(iv) and 5(iv). The reason of this difference is explained by the fact that the 272nd amino acid is Phe in mPPARα-LBD, while that is Ile in hPPARα-LBD. Because of the large steric constraint between the Phe and S-MEHA, S-MEHA in mPPARα-LBD is pushed upward in Fig. 8(k) to change its binding mode. It thus seems that the difference in the 272nd amino acid between human and mouse PPARα-LBDs has an effect on the binding mode of long-chained ligands such as GW409544 and MEHA.

On the other hand, the binding modes of the five types of phthalate esters having an aromatic ring into PPARα-LBDs are remarkably different each other as shown in Fig. 8(a)–(j). Because the sizes of these esters are small, the both *S*- and *R*-forms of these esters can be inserted into the ligand binding pockets of the human and mouse PPARα-LBDs without steric constrain. As for the binding mode of the *S*-form esters, because the steric constrain between these esters and the 272nd amino acid is largely different between the human and mouse PPARα-LBDs, the binding positions of the *S*-form esters are dependent on the type of PPARα-LBDs, as shown in Fig. 8(a), (c), (e), (g) and (i). Accordingly, the 272nd amino acid in the PPARα-LBDs is found to play a considerable role in determining the binding positions of the *S*-form phthalate esters. On the other hand, the binding positions of the *R*-form esters with a short side chain are almost the same in the human and mouse PPARα-LBDs.

We furthermore evaluated the RMSD values between the PPARα-LBD + GW409544 and PPARα-LBD + esters complexes for the human and mouse PPARα-LBDs, in order to make clear the influence of ligand binding on the structures of PPARα-LBDs.

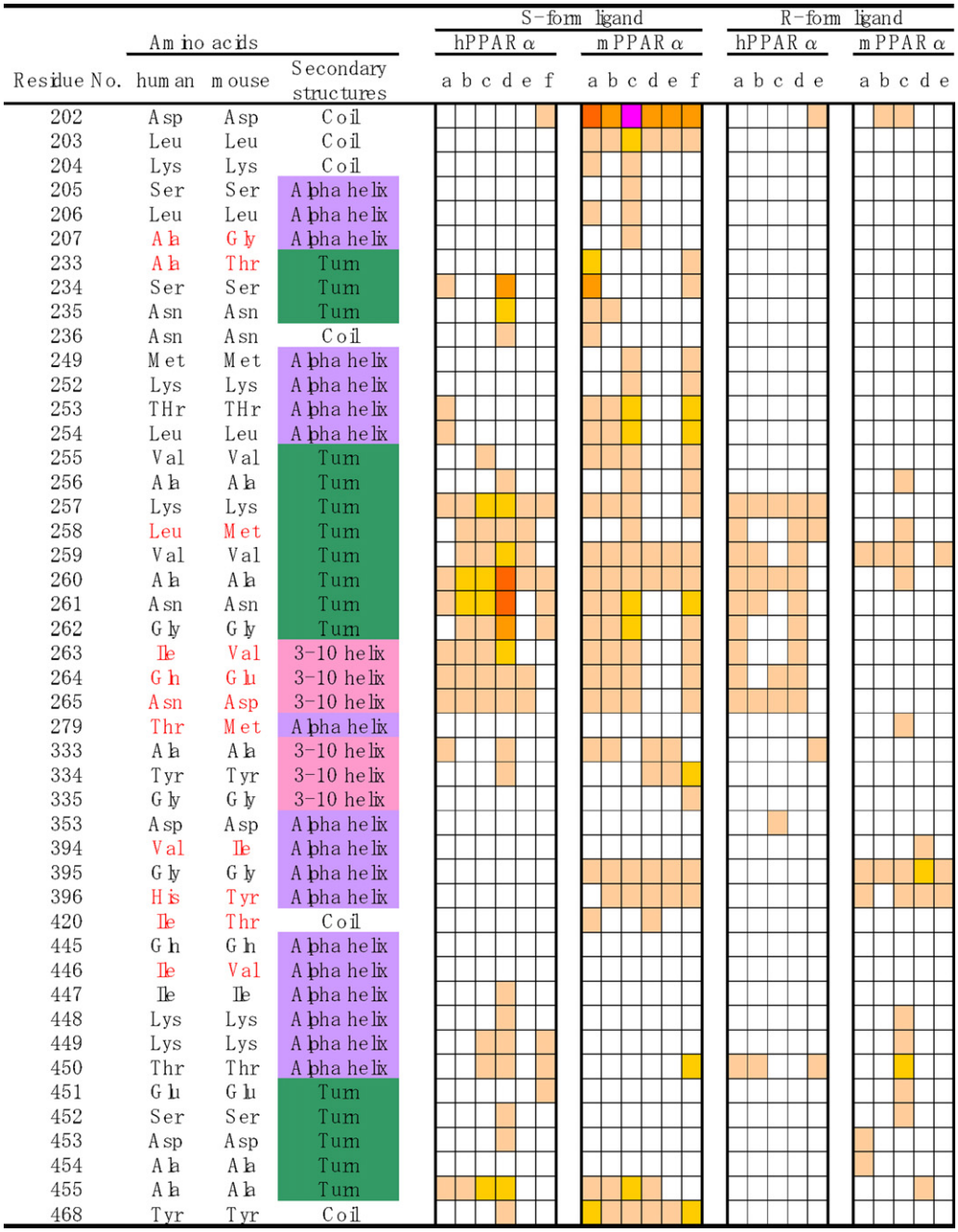

Fig. 9. Change in positions of Cα atoms of human and mouse PPARα-LBDs induced by the binding of the six types of ester ligands: (a) MEP; (b) MBuP; (c) MBeP; (d) MCP; (e) MEHP and (f) MEHA. Based on the structures of PPARα-LBDs + GW409544 complexes, the deviations of Cα atoms are investigated; : deviation is 2.0–3.0 Å, : 3.0–4.0 Å, : 4.0–5.0 Å, : 5.0–6.0 Å, : larger than 6.0 Å. The different amino acids between human and mouse PPARα-LBDs are marked in red. The secondary structures of each amino acid are listed.

In Tables 4(i) and 5(i), the RMSD values for Cα atoms in the PPARα-LBD + esters complexes are compared. The RMSD values for hPPARα-LBD are changed more widely depending on the ester ligands, indicating that the affinity between hPPARα-LBD and ligand depends more largely on the type of ligand molecule.

To elucidate which amino acids of PPARα-LBD are affected largely by the ligand binding, the change in positions of Cα atoms of amino acids was analyzed. Fig. 9 compares these results for the human and mouse PPARα-LBDs bonded with six types of esters. It is found that large structural change over 3 Å is caused at the head part around the 202nd amino acid, the C-terminal 468th one, the turn domains around the 234th and 260th amino acids, and the helix domain around the 395th amino acid. These parts are located at the both ends of LBDs or the turn domains to be more easily affected by the ligand binding.

Fig. 9 also indicates that the *S*-form ligands have larger effect on the LBD structure than the *R*-form ones. It seems that this large effect of the *S*-form is caused by the large steric hindrance between the *S*-form and the ligand-binding pocket. In particular, the binding of *S*-MCP (Fig. 4(d)) changes largely the structure of hPPARα-LBD, because of its sterically bulky side chain.

4.4. Binding properties between PPARα-LBD and ligand molecules

In the present study, we used the semiempirical MO method (PM3 [20]) implemented in the semiempirical MO program

package MOPAC [21] to obtain their electronic properties in solvating water molecules. Furthermore, we calculated the heat of formations for PPARα-LBD, ligand molecule and water molecules for obtaining the binding energy between PPARα-LBD and ligand molecule associated with water molecules. The obtained results by the PM3 method are listed in Tables 4(iv) and 5(iv), indicating that the binding energy between PPARα-LBD and ligand molecule changes at most 51.03 kcal/mol depending on the types of PPAR-LBDs and ligands.

To make clear the reason of this large change in binding energy, we investigated the hydrogen bond lengths between the amino acids of PPARα-LBDs and ligand molecules. In Tables 4(ii) and 5(ii), the amino acids existing near the ligand molecules are listed. As shown in the second column of Table 4(ii), there are 5 hydrogen bonds existing between hPPARα-LBD and GW409544, while only 3 bonds exist between mPPARα-LBD and GW409544. Therefore, the difference in binding energies (−21.05 for human and −14.91 kcal/mol for mouse) can be related with the number of hydrogen bonds between PPARα-LBD and GW409544.

In the previous molecular modeling study [35], the binding characteristic between PPARα and ligands was investigated by considering two kinds of conformations of ligand molecules to find that the binding energies of ligands are dependent on their conformations, resulting in the difference in transfer activation by ligand-addition. It was thus concluded that the conformation of ligand having larger binding energy to PPARα is expected to bind to the ligand binding pocket of PPARα. In the similar way as this study [35], we here considered two forms of ligands and determined which one is more strongly bound to the PPARα-LBDs based on the binding energies obtained by semiempirical MO calculations. The results shown in Tables 4(iv) and 5(iv) indicate that the *R*-forms of the phthalate esters bind more strongly to the human and mouse PPARα-LBDs but for the mPPARα-LBD + MEHP complexes, in which the *S*-form MEHP binds 12 kcal/mol stronger than the *R*-form one. On the other hand, because of the long chain of MEHA, only *S*-form of MEHA can be inserted into the ligand-binding pockets of these PPARα-LBDs.

As for the binding energies of ligands to hPPARα-LBD, we attempted to explain their dependence on the *S*- and *R*-forms of the ligand molecules by the hydrogen bonding structures around the ligand. However, as shown in Tables 4(a)–(iii) and 5(a)–(iii), it was elucidated that the dependence cannot be explained by only the difference in the number of hydrogen bonds between hPPARα-LBD and ligands. For example, in the complexes of hPPARα-LBD + *S*- and *R*-forms of MBeP, the number of hydrogen bonds is 4 for the both forms, whereas the binding energy (−53.87 kcal/mol) of *R*-MBeP is about twice as that (−27.06 kcal/mol) of *S*-MBeP.

On the other hand, the binding strength between mPPARα-LBD and the ester ligands can be qualitatively explained by the hydrogen bonding between mPPARα-LBD and ligands as shown in Tables 4(b)–(iii) and 5(b)–(iii). For example, the binding energies of *S*- and *R*-MEP are −17.44 and −31.00 kcal/mol, respectively. This difference is explained by the difference in the number of hydrogen bonds: 1 (*S*-MEP) and 4 (*R*-MEP). In contrast, the binding energy between mPPARα-LBD and *R*-MBeP is about 6 kcal/mol larger than that of *S*-form MBeP, although the number of hydrogen bonds is the same for the both forms. To make clear the reason of this difference in binding energy, we analyzed the charge distribution of the two oxygen atoms of the COO^- part in MBeP. The averaged charge is −0.588 (*S*-MBeP) and −0.613 (*R*-MBeP), respectively. Therefore, it can be explained that the binding energy of *R*-MBeP is larger than that of *S*-MBeP, because the charge of the COO^- part in *R*-MBeP is negatively larger than that in *S*-MBeP.

4.5. Chemical reactivity of PPARα-LBD + ligand complexes

In order to elucidate the influence of ligand binding on the chemical reactivity of PPARα-LBD, we investigated energy levels and spatial distributions of MOs existing around the HOMO (highest occupied MO) and LUMO (lowest unoccupied MO). Tables 4(v) and 5(v) compare the results for the complexes of human and mouse PPARα-LBDs + GW409544 or ester ligands.

The energy gap between HOMO and LUMO (H–L gap), which is used as an indicator of chemical reactivity, changes in the range between 5.37 (S-MEP) and 6.55 eV (R-MEHP) depending on the bound ligand for the human PPARα-LBD. The variation width of the gap energies for mPPARα-LBD is 5.49–7.16 eV. Therefore, it is expected that the chemical reactivity of mPPARα-LBD is more largely affected by the binding of the ester ligands. It is also noted that the H–L gap (4.97 eV) of the mPPARα-LBD + GW409544 complex is smaller than any other complexes in Tables 4(v) and 5(v), indicating that the mPPARα-LBD + GW409544 complex is more chemically reactive.

To make a prediction for chemically reactive sites, the spatial distributions of HOMO and LUMO were analyzed. Based on the size of the eigenvector coefficients for each atom, the amino acid or ligand with the largest distribution of HOMO or LUMO was assigned and listed in Tables 4(v) and 5(v). The LUMO distribution site can easily accept electron to contribute nucleophilic reactions, while the HOMO distribution site can donate electron to cause

Table 6
Effects of ligand injection on the expression of PPARα-related hepatic enzymes obtained by physiological experiments

Ligands	M.W.[a]	Log *P*[b]	*X* log *P*[b]	PT[c]	PH[c]	VLCAD[c]	TPα[c]	TPβ[c]
No treatment	–	–	–	1.00 ± 0.11[e]	1.00 ± 0.16[e]	1.00 ± 0.08	1.00 ± 0.32	1.00 ± 0.11
DEP[d]	222.24	2.42	2.606	0.98 ± 0.16	1.02 ± 0.01	1.04 ± 0.03	1.32 ± 0.47	1.18 ± 0.18
DBP[d]	278.34	4.50	4.406	1.04 ± 0.26	1.20 ± 0.04[f]	0.92 ± 0.07	1.64 ± 0.19[f]	1.17 ± 0.07
BBP[d]	312.37	4.73	4.821	1.44 ± 0.04[f]	1.16 ± 0.06	0.95 ± 0.05	1.90 ± 0.18[f]	1.32 ± 0.06[f]
DCP[d]	330.42	–	5.624	1.25 ± 0.18	1.08 ± 0.07	0.97 ± 0.04	1.96 ± 0.33[f]	1.34 ± 0.13[f]
DEHP[d]	390.56	7.60	7.644	1.59 ± 0.14[f,g]	1.59 ± 0.06[f,g]	1.22 ± 0.01[f]	2.60 ± 0.28[f]	1.73 ± 0.19[f]
DEHA[d]	370.57	–	6.834	1.31 ± 0.18[f,g]	1.37 ± 0.07[f,g]	1.34 ± 0.07[f]	2.67 ± 0.19[f]	1.78 ± 0.26[f]

[a] Molecular weight.
[b] Log *P*: (octanol–water) data provided to ChemIDplus by Syracuse Research Corporation; *X* log *P*: data provided to PubChem. (Computed following the reference J. Chem. Inf. Comput. Sci. 37 (1997) 615).
[c] PT: peroxisomal thiolasae; PH: peroxisomal bifunctional protein; VLCAD: very-long chain acyl-CoA dehydrogenase; TPα: trifunctional protein α subunit; TPβ: 3-ketoacyl-CoA thiolase.
[d] DEP: diethyl phthalate; DBP: di-*n*-butyl phthalate; BBP: butylbenzyl phthalate; DCP: dicyclohexyl phthalate; DEHP: di-(2-ethylhexyl) phthalate); DEHA: di-(2-ethylhexyl) adipate).
[e] Signals obtained by Western blot analysis were quantified by scanning densitometry, and the average value for the no treatment group is assigned to be 1.0. Each value represents the average value ± S.D. (standard deviation).
[f] Significantly different from "No treatment" ($p < 0.05$).
[g] Significant difference between DEHP and DEHA treatments ($p < 0.05$).

electrophilic reactions. The most remarkable feature in Tables 4(v) and 5(v) is that the LUMO is distributed on H440 amino acid for all complexes but for the mPPARα-LBD + *S*-MBeP complex. This result indicates that the H440 amino acid plays an important role in nucleophilic reactions. As shown in Fig. 6, the H440 amino acid was found to contribute to the specific interaction between hPPARα-LBD and GW409544 ligand in the experiment [9]. H440 is hydrogen bound to the COO^- part of GW409544. The present MO calculations elucidate that the H440 of hPPARα-LBD + ligand complexes is also important in the chemical reactions between the complexes and nucleophilic reagents.

On the other hand, the HOMO distribution sites of the complexes are changed largely depending on the bound ligand. Because the complexes with the *R*-form ligands are more stable than those with the *S*-form ligands as shown in Tables 4(iv) and 5(iv), we discuss here the HOMO distributions for only the complexes with the *R*-form ligands. In these complexes, HOMO distributes on E251 or M467 for hPPARα-LBD, while it distributes on only M467 for mPPARα-LBD. From these HOMO distributions, it is expected that E251 in hPPARα-LBD and M467 in mPPARα-LBD may have some contribution on electrophilic reactions.

4.6. Comparison between physiological properties of PPARα-related enzymes induced by ligand injection and calculated electronic properties for mPPARα-LBD + ester ligands

Various influences of the phthalate esters on hepatic enzymes relevant to PPARα are listed in Table 6. Among these phthalate esters, the effect of DEHP injection is the strongest. The adipate ester (DEHA) also has a similar effect on the expressions of enzymes as DEHP. In fact, both DEHA and DEHP significantly activate the expressions of the peroxisomal enzyme PT as well as the mitochondrial enzymes TPα and TPβ. On the other hand, the influences of the BBP and DCP injections are not so large, and those of DBP and DEP are much smaller than that of DEHP. Table 6 indicates that the expression of these enzymes is activated more largely by the injection of the ligand with larger molecular weight and hydrophobicity (*X* log *P*). Among the six types of ligands used in the present study, DEHP and DEHA have similar effect on the expression of PPARα-related enzymes, although their chemical structures are very different from each other, as shown in Fig. 1; DEHP has an aromatic ring, while DEHA is an aliphatic carboxylic acid ester. Therefore, it seems that the interaction between the aromatic ring of a ligand molecule and the amino acids existing around the binding-pocket of mPPARα-LBD is not so essential for the activation of PPARα-related enzymes expression.

Based on the change in the expression of the PPARα-related enzymes induced by the ligand injections shown in Table 6, the six types of ester ligands can be classified into the following three groups: (1) ligands with large enhancement of expression: DEHP and DEHA; (2) ligands with small enhancement: DEP and DBP; and (3) ligands with moderate enhancement: BBP and DCP. Because BBP is metabolized to MBeP or MBuP in living organisms as shown in Fig. 1, the experimental results for BBP cannot be linked uniquely with the calculated results for the mono-forms of ester ligands. Hereafter, we attempted to make clear what kind of calculated electronic properties can explain the trend of the experimentally obtained enhancement of expression for PPARα-related enzymes.

We first compared the size of binding energy between mPPARα-LBD and ester ligands, which are listed in Tables 4(b)–(iv) and 5(b)–(iv). The energies for the more stable form of each ligand are 40.89 (*R*-MBuP) > 35.08 (*S*-MEHA) > 31.00 (*R*-MEP) > 29.33 (*S*-MEHP) > 19.31 (*R*-MCP) > 11.93 kcal/mol (*R*-MBeP), respectively. Therefore, it was elucidated that the size of binding energy cannot be related with the above mentioned grouping of ester ligands obtained by the physiological experiment.

We then compared the HOMO–LUMO energy gaps for the complexes with the more stable form of ligands. As shown in Tables 4(b)–(v) and 5(b)–(v), the gaps are 7.16 (*S*-MEHP) > 6.24 (*R*-MBeP) > 6.23 (*R*-MCP) > 6.09 (*R*-MBuP) > 5.94 (*S*-MEHA) > 5.82 eV eV (*R*-MEP), respectively. These values except for *S*-MEHA can be related with the experimental results.

To make clear the relation between the calculated and experimental results quantitatively, we analyzed the correlation coefficients between them for the five types of phthalate esters. Table 7 lists the values of the coefficients between the calculated results (binding energies (B.E.) and HOMO–LUMO gap) and the experimentally obtained enhancement of the expression of PPARα-related hepatic enzymes (PT, PH, VLCAD, TPα and TPβ) induced by the injection of the five types of phthalate esters. As for the HOMO–LUMO gaps, we considered the values for the complexes with both the *S*- and *R*-form ligands. Note that the values in the last column of Table 7 were obtained based on the HOMO–LUMO gaps for the more stable complexes with mPPARα-LBD and ligand.

As indicated in Table 7, the correlation coefficients between the binding energies and the enhancement of expression for the five types of enzymes are from 0.11 to 0.71 (*S*-form) and from −0.83 to −0.28 (*R*-form), respectively. It is thus elucidated that the binding energies between mPPARα-LBD and ester ligands obtained by the semiempirical MO calculations have no correlation with the enhancement of expression.

On the other hand, the size of HOMO–LUMO gap has a definite correlation with the enhancement of expression. Although the correlation coefficients for the *S*-form ligands are rather small, these for the *R*-form ligands are from 0.72 to 0.99 and large enough for confirming the correlation. Furthermore, based on the binding energies for the *S*- and *R*-forms, we determined the more stable complexes for the five types of ligands and investigated the correlation coefficients between their HOMO–LUMO gaps and the enhancement of expression. As the result, the coefficients became larger to be from 0.79 to 0.98, as shown in the last column of Table 7. Accordingly, it can be concluded that the HOMO–LUMO gaps for more stable complexes with mPPARα-LBD and the phthalate esters have a clear correlation with the enhancement of expression induced by the injection of these esters.

The final goal of our study is to make clear the influence of the ligand injections on the expression of the PPARα-related enzymes for human bodies. Based on the results for the mPPARα-LBD + ligands shown in Table 7 and the HOMO–LUMO gaps for the hPPARα-LBD + ligands, we predicted the influence of ligand

Table 7
Correlation coefficients between the calculated results (HOMO–LUMO gap and biding energies (B.E.)) and the experimentally obtained enhancement of the expression of PPARα-related hepatic enzymes (PT, PH, VLCAD, TPα and TPβ) induced by the injection of phthalate esters shown in Fig. 1

Properties	B.E.		H–L gap		H–L gap
Ligand form	*S*	*R*	*S*	*R*	Stable[f]
Average	0.45	−0.53	0.37	0.90	0.91
PT[a]	0.11	−0.83	0.11	0.90	0.87
PH[b]	0.71	−0.28	0.63	0.93	0.96
VLCAD[c]	0.68	−0.33	0.58	0.72	0.79
TPα[d]	0.31	−0.61	0.19	0.99	0.97
TPβ[e]	0.44	−0.60	0.33	0.96	0.98

[a] PT: peroxisomal thiolasae.
[b] PH: peroxisomal bifunctional protein.
[c] VLCAD: very-long chain acyl-CoA dehydrogenase.
[d] TPα: trifunctional protein α subunit.
[e] TPβ: 3-ketoacyl-CoA thiolase.
[f] H–L gaps for more stable forms of ligands.

injection into human bodies. As shown in Tables 4(a)–(v) and 5(a)–(v), the HOMO–LUMO gaps of the complexes with hPPARα-LBD + ligands are 6.55 (*R*-MEHP) > 6.16 (*R*-MBeP) > 5.93 (*R*-MEP) > 5.92 (*R*-MCP) > 5.82 eV (*R*-MBuP), respectively. Therefore, it is expected that the injection of MEHP into human bodies has the largest enhancement of the expression for the hPPARα-related enzymes. The difference in physiological and electronic properties among the human, mouse and rat PPARα-LBDs are investigating now, and these results will be shown elsewhere.

5. Conclusions

We have investigated the stable structures and their electronic properties of the complexes with human and mouse PPARα-LBDs and the six types of esters as well as GW409544 ligands by using the classical molecular mechanics (MM) and semiempirical molecular orbital (MO) methods. Furthermore, to elucidate the influence of these esters in vivo, we injected them into male mice and observed the change in the expression of PPARα-related enzymes. The comparison between the calculated and observed results elucidates the following points.

1. The structure of the hPPARα-LBD + GW409544 complex obtained by the present study is comparable to the X-ray crystal structure [9] within the 1.53 Å RMSD, indicating that the present MM optimization method in water is applicable for investigating the structure of the complex with PPARα-LBD and other ligands.
2. The obtained binding energies between PPARα-LBDs and two forms (*S*- and *R*-forms) of ester ligands indicate that the *R*-form ligands bind more strongly than the *S*-form ones to the ligand-binding pocket of human and mouse PPARα-LBDs.
3. The experimentally obtained enhancement in expression of the mPPARα-related enzymes induced by the injection of phthalate esters can be related with the calculated HOMO–LUMO energy gaps for the complexes with mPPARα-LBD and phthalate esters.

Acknowledgments

This work was supported in part by the grants from CASIO Science Promotion Foundation, Kayamori Foundation of Informational Science Advancement and Toukai Foundation for Technology.

Appendix A. Supplementary data

Supplementary data associated with this article can be found, in the online version, at doi:10.1016/j.jmgm.2008.02.003.

References

[1] E.A. Lock, A.M. Mitchell, C.R. Elcombe, Biochemical mechanisms of induction of hepatic peroxisome proliferation, Annu. Rev. Pharmacol. Toxicol. 29 (1989) 145–163.
[2] J.K. Reddy, D.L. Azarnoff, C.E. Hignite, Hypolipidaemic hepatic peroxisome proliferators form a novel class of chemical carcinogens, Nature 283 (1980) 397–398.
[3] S. Mandard, M. Muller, S. Kersten, Peroxisome proliferator-activated receptor alpha target genes, Cell. Mol. Life Sci. 61 (2004) 393–416.
[4] P.R. Devchand, H. Keller, J.M. Peters, M. Vazquez, F.J. Gonzalez, The PPARalpha-leukotriene B4 pathway to inflammation control, Nature 384 (1996) 39–43.
[5] M. Iglarz, R.M. Touyz, E.C. Viel, P. Paradis, F. Amiri, Q.N. Diep, E.L. Schiffrin, Peroxisome proliferator-activated receptor-alpha and receptor-gamma activators prevent cardiac fibrosis in mineralocorticoid-dependent hypertension, Hypertension 42 (2003) 737–743.
[6] C.H. Lee, P. Olson, R.M. Evans, Minireview: lipid metabolism, metabolic diseases, and peroxisome proliferator-activated receptors, Endocrinology 144 (2003) 2201–2207.
[7] J.M. Peters, R.C. Cattley, F.J. Gonzalez, Role of PPAR alpha in the mechanism of action of the nongenotoxic carcinogen and peroxisome proliferator Wy-14,643, Carcinogenesis 18 (1997) 2029–2033.
[8] S. Kersten, W. Wahli, Peroxisome proliferator activated receptor agonists, EXS 89 (2000) 141–151.
[9] H.E. Xu, M.H. Lambert, V.G. Montana, K.D. Plunket, L.B. Moore, J.L. Collins, J.A. Oplinger, S.A. Kliewer, R.T. Gampe Jr., D.D. McKee, J.T. Moore, T.M. Willson, Structural determinants of ligand binding selectivity between the peroxisome proliferator-activated receptors, Proc. Natl. Acad. Sci. U.S.A. 98 (2001) 13919–13924.
[10] P. Cronet, J.F. Petersen, R. Folmer, N. Blomberg, K. Sjöblom, U. Karlsson, E.L. Lindstedt, K. Bamberg, Structure of the PPARalpha and -gamma ligand binding domain in complex with AZ 242; ligand selectivity and agonist activation in the PPAR family, Structure 9 (2001) 699–706.
[11] HyperChem, version 6.03, 2000, Hyper cube, Inc., Florida, USA.
[12] W.D. Cornell, P. Cieplak, C.I. Bayly, I.R. Gould, K.M. Merz, D.M. Ferguson Jr., D.C. Spellmeyer, T. Fox, J.W. Caldwell, P.A. Kollman, A second generation force field for the simulation of proteins, nucleic acids and organic molecules, J. Am. Chem. Soc. 117 (1995) 5179–5197.
[13] D.F.V. Lewis, M.N. Jacobs, M. Dickins, B.G. Lake, Molecular modeling of the peroxisome proliferator-activated receptor alpha (PPAR alpha) from human, rat and mouse, based on homology with the human PPAR gamma crystal structure, Toxicol. In Vitro 16 (2002) 275–280.
[14] B.G. Lake, J.C. Phillips, J.C. Linnell, S.D. Gangolli, The in vitro hydrolysis of some phthalate diesters by hepatic and intestinal preparations from various species, Toxicol. Appl. Pharmacol. 39 (1977) 239–248.
[15] N.G. Coldham, M. Dave, M.J. Sauer, Analysis of di-*n*-butylphthalate biotransformation in cattle by liquid chromatography/ion trap mass spectrometry/mass spectrometry, J. Mass Spectrom. 33 (1998) 803–810.
[16] D.A. Eigenberg, H.P. Bozigian, D.E. Carter, I.G. Sipes, Distribution, excretion, and metabolism of butylbenzyl phthalate in the rat, J. Toxicol. Environ. Health 17 (1986) 445–456.
[17] H. Lygre, E. Solheim, N.R. Gjerdet, Leaching from denture base materials in vitro, Acta Odontol. Scand. 53 (1995) 75–80.
[18] P.W. Albro, S.R. Lavenhar, Metabolism of di(2-ethylhexyl)phthalate, Drug Metab. Rev. 21 (1989) 13–34.
[19] T. Takahashi, A. Tanaka, T. Yamaha, Elimination, distribution and metabolism of di-(2-ethylhexyl)adipate (DEHA) in rats, Toxicology 22 (1981) 223–233.
[20] J.J.P. Stewart, Optimization of parameters for semi-empirical methods: I-method, J. Comput. Chem. 10 (1989) 209–220.
[21] J.J.P. Stewart, MOPAC2000, Fujitsu, Tokyo, Japan, 1999.
[22] M.J. Frisch, et al., Gaussian 03, Revision B.04, Gaussian, Inc., Pittsburgh, USA, 2003
[23] C. Moller, M.S. Plesset, Note on an approximation treatment for many-electron systems, Phys. Rev. 46 (1934) 618–622.
[24] B.H. Besler, K.M. Merz Jr., P.A. Kollman, Atomic charges derived from semiempirical methods, J. Comput. Chem. 11 (1990) 431–439.
[25] P. Cieplak, W.D. Cornell, C. Bayly, P.A. Kollman, Application of the multimolecule and multiconformational RESP methodology to biopolymers: charge derivation for DNA, RNA and proteins, J. Comput. Chem. 16 (1995) 1357–1377.
[26] TINKER, version 3.9, 1990, Jay William Ponder, http://dasher.wustl.edu/tinker/.
[27] D. Qiu, P.S. Shenkin, F.P. Hollinger, W.C. Still, The GB/SA continuum model for salvation. A fast analytical method for the calculation of approximate Boron radii, J. Phys. Chem. A 101 (1997) 3005–3014.
[28] A. Klamt, G. Schuurmann, COSMO: a new approach to dielectric screening in solvents with explicit expressions for the screening energy and its gradient, J. Chem. Soc., Perkin Trans. 2 (1993) 799–805.
[29] T. Aoyama, J.M. Peters, N. Iritani, T. Nakajima, K. Furihata, T. Hashimoto, F.J. Gonzalez, Altered constitutive expression of fatty acid-metabolizing enzymes in mice lacking the peroxisome proliferator-activated receptor alpha (PPARalpha), J. Biol. Chem. 273 (1998) 5678–5684.
[30] T. Nakajima, Y. Kamijo, N. Usuda, Y. Liang, Y. Fukushima, K. Kametani, F.J. Gonzalez, T. Aoyama, Sex-dependent regulation of hepatic peroxisome proliferation in mice by trichloroethylene via peroxisome proliferator-activated receptor alpha (PPARalpha), Carcinogenesis 21 (2000) 677–682.
[31] S. Miyazawa, T. Osumi, T. Hashimoto, The presence of a new 3-oxoacyl-CoA thiolase in rat liver peroxisomes, Eur. J. Biochem. 103 (1980) 589–596.
[32] T. Osumi, T. Hashimoto, Purification and properties of mitochondrial and peroxisomal 3-hydroxyacyl-CoA dehydrogenase from rat liver, Arch. Biochem. Biophys. 203 (1980) 372–383.
[33] K. Izai, Y. Uchida, T. Orii, S. Yamamoto, T. Hashimoto, Novel fatty acid beta-oxidation enzymes in rat liver mitochondria. Part I. Purification and properties of very-long-chain acyl-coenzyme A dehydroge nase, J. Biol. Chem. 267 (1992) 1027–1033.
[34] Y. Uchida, K. Izai, T. Orii, T. Hashimoto, Novel fatty acid beta-oxidation enzymes in rat liver mitochondria. Part II. Purification and properties of enoyl-coenzyme A (CoA) hydratase/3-hydroxyacyl-CoA dehydrogenase/3-ketoacyl-CoA thiolase trifunctional protein, J. Biol. Chem. 267 (1992) 1034–1041.
[35] H. Uchiki, H. Miyachi, Molecular modeling study of species-selective peroxisome proliferator-activated receptor (PPAR) alpha agonist; possible mechanism(s) of human PPARalpha selectivity of an alpha-substituted phenylpropanoic acid derivative (KCL), Chem. Pharm. Bull. 52 (2004) 365–367.